Environmental Fluid Mechanics
https://doi.org/10.1007/s10652-022-09894-x

ORIGINAL ARTICLE

Dense pulses formed from fissioning internal waves

Samuel G. Hartharn-Evans[1] · **Marek Stastna**[2] · **Magda Carr**[1]

Received: 28 January 2022 / Accepted: 1 September 2022

Abstract
Cold pulses generated by the fission of internal solitary waves over gentle slopes are an important source of nutrients and relief from excess heat to benthic ecosystems. This numerical study investigates the effect of stratification form on pulses produced by fission of internal solitary waves propagating over a smooth, gentle, linear topographic slope in 2D simulations. Three stratification types are investigated, namely (i) thin tanh (homogeneous upper and lower layers separated by a thin pycnocline), (ii) surface stratification (linearly stratified layer overlaying a homogeneous lower layer) and (iii) broad tanh (continuous density gradient throughout the water column). Incident wave amplitude was varied. In the thin tanh stratification, good agreement is seen with past studies, whilst the dynamics observed in the surface stratification are very similar to those in the thin tanh stratification. However, in the broad tanh stratification, due to the different form of incident waves, the fission dynamics differ, but produce pulses similar in form to those produced by fission in the other stratifications. Pulse amplitude, wavelength and propagation velocity are found to strongly depend on incident wave amplitude, and each degenerate linearly as the pulse propagates upslope.

Keywords Bolus/pulse · Internal solitary wave · Fission · Topographic effects

1 Introduction

In the ocean, vertical variation in seawater temperature and salinity acts to stratify the oceanic water column, producing conditions in which density disturbances can propagate along a pycnocline as internal waves. Internal solitary waves (ISWs) are a particular form of internal waves that have amplitude comparable to the pycnocline thickness, and often the overall depth of the water column [e.g. 1]. Whilst propagating over a flat

✉ Samuel G. Hartharn-Evans
s.hartharn-evans2@newcastle.ac.uk

Marek Stastna
mmstastna@uwaterloo.ca

Magda Carr
magda.carr@newcastle.ac.uk

[1] School of Mathematics, Statistics and Physics, Newcastle University, Newcastle NE1 7RU, UK

[2] Department of Applied Mathematics, University of Waterloo, Waterloo, ON, Canada

Published online: 16 September 2022

bottom in deep water, ISWs can travel long distances without change of form. However, as ISWs move into shallower waters, the bed interacts with the flow, and waves propagating over shallowing topography undergo shoaling. During shoaling, the form of ISWs change considerably, and they are known to modify water properties by inducing considerable vertical mixing of cool, nutrient rich waters from depth [2, 3]. These changes can benefit benthic ecosystems such as coral reefs and kelp forests [4], and may increase reef resilience to climate change by increasing high frequency temperature variability [2, 5].

ISWs are found commonly across the world's oceans, and they maintain high levels of research interest due to their effectiveness in transporting energy and water masses (and their associated heat, nutrients and sediments) [6], and for mixing in the ocean [e.g. 7, 8, 9]. Typically, internal waves are generated on density interfaces in stably-stratified fluids by barotropic motion over topography such as sills, slopes and the shelf edge [e.g. 10, 11, 12]. They are characterised by a balance of nonlinear steepening and wave dispersion, and as a result are able to travel large distances without significant change of form or magnitude.

Whilst field observations of ISWs document the complexity of real-world dynamics, practical and technological constraints often limit the spatial and temporal resolution of field observations. Instead, idealised modelling studies at the laboratory scale allow full understanding of the underlying fluid dynamics, and the alteration of various parameters to identify trends and regimes that represent specific dynamical characteristics. Numerous efforts have been made to study the dynamics of shoaling mode 1 ISWs of depression on a range of idealised linear (and mostly steep) slopes in laboratory experiments [e.g. 13] ($s = 0.1 - 0.15$), [14] ($s = 0.069 - 0.214$), and [15] ($s = 0.143 - 0.417$), and numerical models [e.g. 16] ($s = 0.01 - 0.3$), [17] ($s = 0.03 - 0.3$), [18] ($s = 0.218$) [19] ($s = 0.02$) where s is the vertical displacement per unit horizontal displacement. Whilst these studies have investigated shoaling over a range of slopes (up to $s = 0.417$), geophysical slopes are very mild, $s \approx 0.001$ for the coastal ocean, $s \approx 0.01$ for lakes, and $s = 0.03 - 0.07$ for typical continental shelves [20], milder than the slopes in most previous studies.

Laboratory experiments [e.g. 21], numerical simulations [e.g. 19] and field observations [e.g. 22, 23, 24] have shown that as ISWs of depression shoal over geophysically representative mild slopes they undergo a process called fission. In fissioning waves, nonlinear steepening is insufficient to cause overturning of the wave [16], and instead, as the back of the wave steepens, the leading wave evolves into a train of internal bores (ISWs of elevation with strongest currents and temperature fronts near the bed) or boluses [2, 25]. Whilst Xu and Stastna [19] recently investigated the role of boundary layer instability in fissioning waves propagating over realistic slopes in a high resolution model, there is very little published research into the bottom boundary layer (BBL) dynamics during fissioning [7]. When shoaling, energy transported by ISWs is used to enhance turbulent, irreversible mixing [26]. This process extends over a large area, in the New Jersey shelf, where it has been observed over a distance of 35 km [27].

To date, all laboratory scale studies of ISWs shoaling over slopes gentle enough for fission to occur have been for a three-layer stratification with a homogeneous surface and bottom layer, separated by a thin pycnocline, resembling an idealised three-layer ocean [e.g. 16, 19, 17, 28, 29]. Whilst some ISW shoaling studies have investigated different stratifications (with the pycnocline centre at mid-depth, and varying pycnocline thicknesses [30, 31]), these have been restricted to steeper slopes, over which fission does not occur. As a result, no studies deviating from a three-layer stratification have investigated wave fission, despite these mild slopes being most representative of the real ocean.

Ocean stratification can be described by the density field, ρ which can be expressed as a function of depth z via a hyperbolic tangent profile, and for this reason is widely used in numerical and laboratory studies [e.g. 31, 32, 30],

$$\rho(z) = \rho_0 + \Delta\rho \tanh\left(\frac{z - z_{pyc}}{h_{pyc}}\right), \tag{1}$$

where ρ_0 is the density of the lower layer, $\Delta\rho$ the change in density through the water column, z_{pyc} the depth of the centre of the pycnocline, and h_{pyc} the pycnocline half thickness.

The thin tanh profile system represents a lower limit of h_{pyc}. Yet, stratification in the real-world ocean varies, with associated variability in h_{pyc}. For example, the Labrador Sea is well represented by the three layer idealised system, whilst in the Sulu Sea, density varies linearly with depth over the entire upper layer, so a broader pycnocline is more representative [33]. Focusing on steeper slopes, previous work investigated the role of varying stratification on shoaling dynamics [34], identifying that dependent on the location of density gradients in the stratification, different shoaling behaviours were suppressed. Past studies of the field have also identified the role of seasonal variation in offshore stratification (as a result of upwelling) in influencing the behaviour of bores [35, 36]. With such a variation in pycnocline thickness in the real ocean, it is reasonable to question what impact stratification form may have on fission dynamics. In this paper, three stratification types are investigated, namely (i) thin tanh (homogeneous upper and lower layers separated by a thin pycnocline), (ii) surface stratification (linearly stratified layer overlaying a homogeneous lower layer) and (iii) broad tanh (continuous density gradient throughout the water column). For the first time, ISW fissioning is investigated in detail in the surface and broad tanh stratification cases using numerical modelling. During the fission process, pulses of dense fluid are formed that travel upslope, this paper focuses on investigating changes to these pulses of dense fluid (hereafter referred to simply as "pulses"), and pulse structure and transport of lower-layer fluid.

Use of numerical simulations is made to investigate the propagation of a mode-1 ISW of depression propagating over a uniformly sloping solid boundary. Results are presented to aid comparison between field observations such as static temperature loggers, and these numerical simulations.

The paper is organised as follows. In Sect. 2 the numerical methods are described. In Sect. 3.1, the formation and structure of pulses are described, followed by a description of the evolution and degeneration in Sect. 3.2. Finally, a discussion of these results, and their relevance to the ocean scale, as well as conclusions are given in Sect. 4.

2 Methods

ISWs were simulated in a rectangular tank with waves initiated using the lock gate technique, with the same simulation setup to the extended tank described in [34]. A schematic of the model set-up is given in Fig. 1a, where the length of the tank $L_x = 14.5$ m, and the depth of the tank $L_z = 0.3$ m. A hyperbolic smoothing function produces a numerical step in density 0.3 m from the left end of the tank, from which an ISW is produced propagating from left to right.

Simulations were carried out with the pseudospectral code SPINS described in Subich et al [37] in two-dimensions. The code has been thoroughly validated using physical laboratory experiments in a number of different configurations including boundary layer

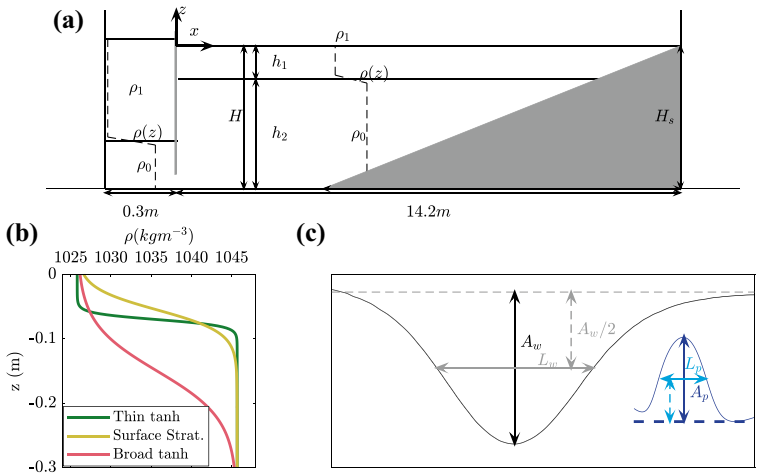

Fig. 1 **a** Schematic diagram of numerical domain used throughout this study, **b** profiles from each of the three stratification types used in the corresponding numerical models (solid lines), and **c** the definitions for wave properties A_w and L_w, and pulse properties (blue) A_p and L_p

instabilities [e.g. 38], interaction with topography [e.g. 39], and shoaling [e.g. 34]. It is available for download through its online manual:

https://wiki.math.uwaterloo.ca/fluidswiki/index.php?title=SPINS_User_Guide

The model solves the stratified Navier–Stokes equations subject to the Boussinesq approximation:

$$\frac{\partial \vec{u}}{\partial t} + \vec{u} \cdot \vec{\nabla}\vec{u} = -\frac{1}{\rho_0}\vec{\nabla}P + \nu\nabla^2\vec{u} - \frac{\rho g}{\rho_0}\hat{k}, \tag{2}$$

$$\vec{\nabla} \cdot \vec{u} = 0, \tag{3}$$

$$\frac{\partial \rho}{\partial t} + \vec{u} \cdot \vec{\nabla}\rho = \kappa \nabla^2 \rho, \tag{4}$$

where $\vec{u}$ is the velocity, t is time, P is the pressure, ρ is the density and ρ_0 is some reference density of the fluid (here $\rho_0 = 1026$ kg m^{-3}). The physical parameters are gravity g (set at 9.81 ms^{-2}), the shear viscosity ν (set at 10^{-6} m^{2}s^{-1}, chosen to be consistent with the physical value) and scalar diffusivity κ (set at 10^{-7} m^{2}s^{-1}). The unit vector in the vertical direction is denoted by $\hat{k}$. No slip boundary conditions were applied at the flat upper, and mapped lower boundaries to satisfy model requirements. A mapped Chebyshev grid is employed in the vertical, implying a clustering of points near both the upper and lower boundary that scales with the number of points in the vertical squared, and that vertical resolution improves over the slope. Free-slip boundary conditions were applied at the vertically oriented left and right ends of the computational domain, the grid spacing of which was regularly spaced. Grid resolution was 4096 points in the x and 256 grid points in the z coordinate, giving $dx = 3.5$ mm, and away from the slope, dz varies between 0.124 mm in the BBL and 1.8 mm near mid-depth. Sensitivity experiments and double and half resolution indicate flow features are appropriately resolved and robust at this resolution, except in

the thin tanh stratification. Following these simulations, the horizontal grid resolution was doubled (to 8192 points in the x) for the four largest amplitude wave thin tanh stratification experiments (Thin-7 L, Thin-10 L, Thin-20 L, Thin-30 L).

The hyperbolic tangent profile in Eq. 1 was employed for the three stratification types (Fig. 1b), namely, (i) a system like that studied previously in the literature consisting of a thin, linearly stratified pycnocline sandwiched between homogeneous layers, here referred to as "thin tanh stratification" (ii) a stratification consisting of a homogeneous bottom layer and an approximately linearly stratified top layer, here referred to as "surface stratification", as the density gradient is close to the surface and (iii) a water column in which the density varies linearly with depth throughout the full water depth, here referred to as "broad tanh stratification", due to the large value of h_{pyc}. Fourteen model runs are presented in this study (see Table 1) representing five initial wave amplitudes in each of the three stratification types (except for the Broad tanh stratification, where four different wave amplitudes are simulated). All simulations are carried out for a slope of $s = 0.033$, and the bottom boundary follows the form of Lamb and Nguyen [40]:

$$z = s\big(\text{itanh}(x, L_x - L_s, d) - \text{itanh}(x, L_x, d)\big) \tag{5}$$

where

$$\text{itanh}(x, a, d) = \frac{1}{2}\left(x - a + d\ln\left(2\cosh\left(\frac{x-a}{d}\right)\right)\right) \tag{6}$$

and d (= 0.03) represents a characteristic distance for the transition from 0 to a constant slope of 1, and L_s the length of the slope (9 m). The function smooths the transition from the flat bed to the slope, which is necessary for the spectral code.

Dense pulses formed by the fission process were identified using the Matlab peak fitting function to find peaks in the depth of the $\rho = \rho_0 + \Delta\rho/2$ contour (which represents the centre of the pycnocline in each case). Peaks related to each pulse were identified

Table 1 Summary of simulation parameters. A_w, L_w and c are incident wave amplitude, wavelength and propagation speed respectively (see Fig. 1c), h_{adj_pyc} is the location of the centre of the pycnocline behind the gate

Simulation Name	Stratification Type	h_{adj_pyc} (m)	A_w (m)	L_w (m)	c (m/s)
Broad-5L	Broad tanh	0.1682	0.010	0.358	0.083
Broad-10L	Broad tanh	0.2237	0.035	0.386	0.081
Broad-20L	Broad tanh	0.2541	0.046	0.412	0.079
Broad-30L	Broad tanh	0.2926	0.054	0.429	0.079
Surface-5L	Surface	0.0732	0.011	0.541	0.078
Surface-7L	Surface	0.1000	0.028	0.501	0.086
Surface-10L	Surface	0.1287	0.045	0.504	0.092
Surface-20L	Surface	0.1591	0.061	0.533	0.097
Surface-30L	Surface	0.1968	0.077	0.599	0.097
Thin-5L	Thin tanh	0.0855	0.009	0.646	0.095
Thin-7L	Thin tanh	0.1242	0.031	0.573	0.104
Thin-10L	Thin tanh	0.1568	0.048	0.600	0.108
Thin-20L	Thin tanh	0.1908	0.063	0.668	0.110
Thin-30L	Thin tanh	0.2321	0.075	0.791	0.114

manually, and the amplitude(A_p), wavelength (λ_p), and propagation speed (c_p) calculated in the same manner as for wave amplitude, wavelength and propagation speed (Fig. 1a).

3 Results

A summary of the dynamics of a fissioning ISW is described in this section. Examples displayed in this section show the surface and broad stratifications, which have not previously been described in the existing literature. Numerical simulations in the thin tanh are qualitatively similar to those in the surface stratification. High resolution simulations of fissioning ISWs in a thin tanh stratification are described in detail in Xu and Stastna [19]. Throughout this text, the features formed by fission are referred to as "pulses" reflecting the terminology commonly used for field observations.

3.1 Initial pulse formation

After the initialisation of each simulation in the surface and thin tanh stratification, an ISW of depression is formed after a small sorting distance (of approximately 1 m). The ISW of depression propagates along the flat bed of the tank until it reaches the toe of the slope at $x = 4.9$ m. On reaching the slope, the ISW continues to propagates upslope a distance without significant change of form. However, around halfway up the slope (at $x = 9.5$ m), the wave shape begins to adjust to the evolving water depth, becoming a long wave with a shallow front face that aligns itself to the topographic slope, and a steepening rear face (see Fig. 2a, f). During this process, reverse flow at the bed due to BBL separation occurs [41] (indicated in Fig. 2a by a red (positive velocity) region around $x = 9.5$ m). The flow reversal begins to grow, as isopycnals at the rear face of the wave rise above the resting pycnocline depth (referred to in other literature [e.g. 16] as a positive tail), indicating the formation of the first wave of elevation (Fig. 2b, g). Whilst the propagation of the long wave of depression is almost halted, this wave emerges from the rear face of the long wave with the signal of an internal wave of elevation at the lower boundary in the velocity and vorticity (a smooth bump of positive velocity and negative vorticity, Fig. 2b-inset), and continues to propagate upslope as a pulse of dense fluid (Fig. 2h–j). These pulses transport dense, lower layer fluid upslope (Fig. 5d, e) above it's resting height. This role of BBL dynamics in the formation of the ISWs of elevation was previously identified in Xu and Stastna [19], where the ability of a separation bubble to form in the footprint of the ISW of elevation (which requires an adverse background current) is due to the residual current induced by the leading ISW of depression (Fig. 2a–c). As the rear face of the first pulse clears the trough of the long wave, a second pulse is formed at the rear face in the same process (Fig. 2c, inset) and also propagates upslope (Fig. 2d, i). Horizontal fluid velocities in the pulse are in the upslope direction (red), which is opposite to flow directly under the leading long wave at the BBL. These results for the surface stratification are qualitatively similar to the thin tanh stratification simulations in this study, as well as prior high resolution simulations of Xu and Stastna [19] and experimental observations of Ghassemi et al [28] for the thin tanh stratification. In addition, the dynamics are comparable to an experimental observation of the emergence of fissioning dynamics in the surface stratification [34].

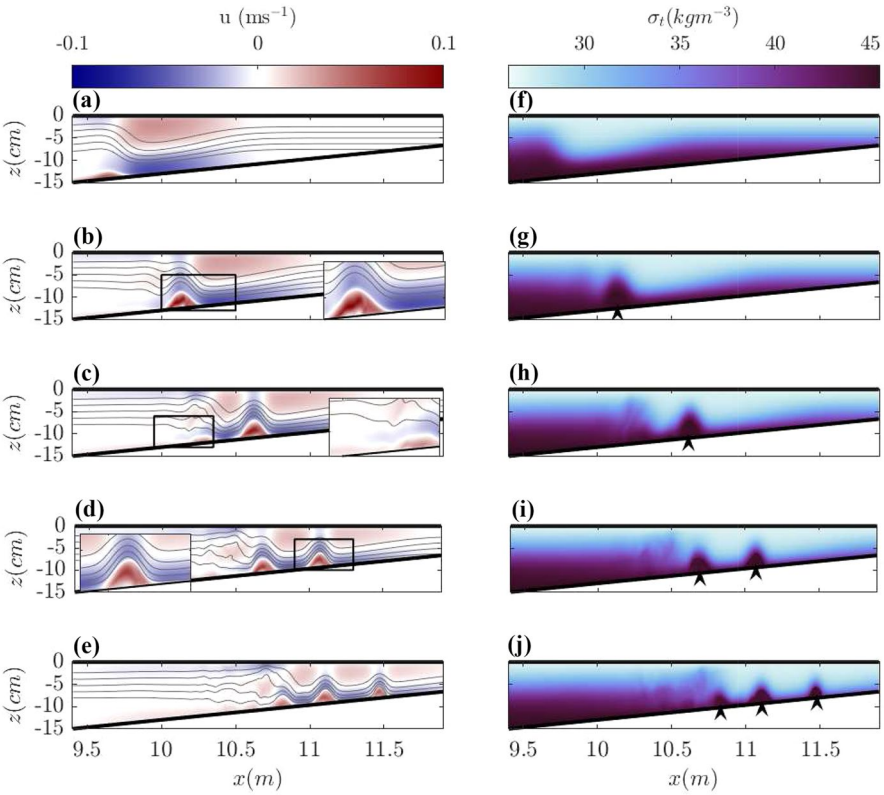

Fig. 2 Time sequence showing an example fissioning wave in the surface stratification (Exp. Surface-10L). Left panels **a**–**e** showing horizontal velocity, u, overlaid with isopycnals (in black), and right panels **f**–**j** showing density ($\sigma_t = \rho - 1000$). Black arrows indicate the location of the pulse, time interval between images is $\Delta t = 10$s

These similarities are expected, given the similarity of the stratification throughout the lower layer to the thin tanh case, and in particular close to the bottom boundary, where the key dynamics involved in fissioning occur (Fig. 1 b).

In the surface and thin tanh stratifications, as incident wave amplitude increases, the fission process becomes more unstable. For large incident waves, a global instability (an instability that is strongly coherent in space and time (e.g. Bogucki and Redekopp, 1999; Carr et al, 2008), forms from the separation bubble. The global instability manifests itself as coherent patches of vorticity which are shed upwards from the separation bubble and follow the wave form as it shoals (Fig. 3e–g, blue arrow). This causes turbulent motion at the pycnocline, and around the pulse (Fig. 3c–d). Global instabilities have previously been linked to sediment resuspension and enhanced turbulent kinetic energy under ISWs of depression in field observations Bogucki et al [42]. These vortices may not only contribute to loss of energy from the incident ISW of depression, but could also contribute to loss of energy and mass from the pulses (see Sect. 3.2, Fig. 9), with large vortices shed from the rear face of the leading pulse (e.g. Fig. 3c, g , black arrow).

In the broad tanh stratification, the incident wave approaching the slope is in the form of a train of large amplitude waves, which alternate between waves of elevation and waves

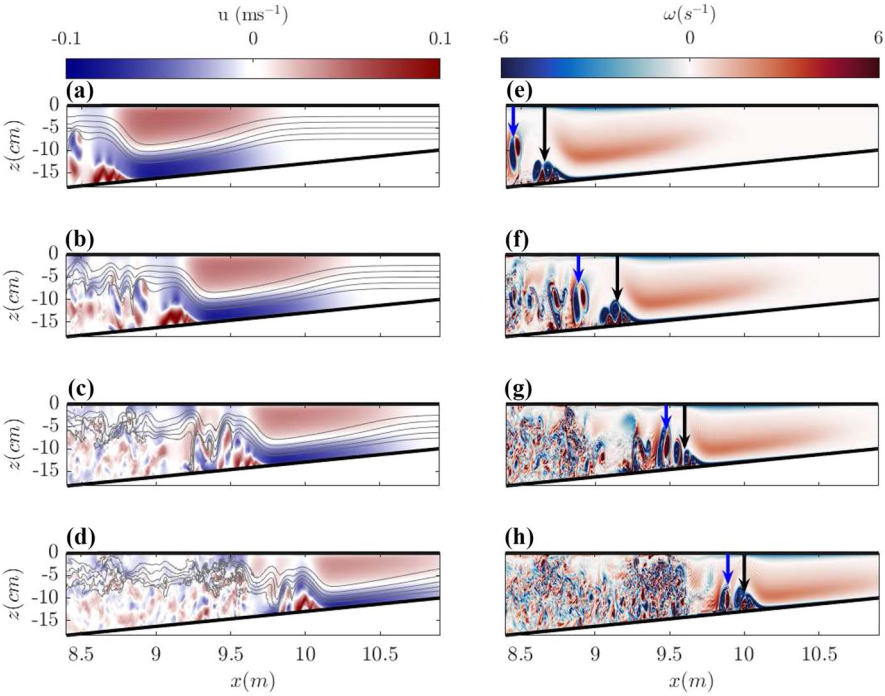

Fig. 3 Time sequence for a turbulent fissioning wave in the surface stratification (Exp. Surface-30L). Left panels **a**–**d** showing horizontal velocity, u, overlaid with isopycnals (in black), and right panels **e**–**h** showing vorticity. Time interval between images is $\Delta t = 8s$. In panels **e**–**h**, the black and blue arrows indicate the location of the separation bubble and shed vortices respectively

of depression (Fig. 4a, b), compared to the single incident ISW of depression in the other stratifications (e.g. Fig. 2a). As a result, whilst the process of ISW fission is very similar in the surface and thin tanh stratifications (where the pycnocline is vertically offset from the mid-depth of the tank), in the broad tanh stratification, the process of wave fission is considerably different. Whilst separation of the boundary layer still occurs under the rear part of the leading wave of depression, the subsequent flow reversal is enhanced by the wave of elevation directly above it (Fig. 4b). In the broad stratification, as the wave propagates upslope, the first incident wave of elevation steepens on both the rear and leading front, until a pulse emerges from this wave, with a velocity structure resembling an ISW of elevation (Fig. 4c), leaving behind the leading wave with much reduced amplitude (Fig. 4d). In the example simulation, the second and third pulses form simultaneously, one emerging from the second approaching wave of elevation, and one emerging from the remnants of the initial incident wave of elevation. Each pulse propagates upslope, bringing a volume of dense fluid far upslope, beyond its undisturbed height (Figs. 4f, 5f). The velocity structure of these pulses resemble closely those in the thin tanh and surface stratifications (Fig. 4d c.f. Fig. 2c), despite the differences in the incident waves. However, in the broad tanh regime, even the largest pulses (produced by fission of larger amplitude incident waves) remain stable and laminar.

The upslope transport of lower layer fluid may be indicated by the number of dense pulses propagating upslope, along with their size (amplitudes and wavelengths), and so

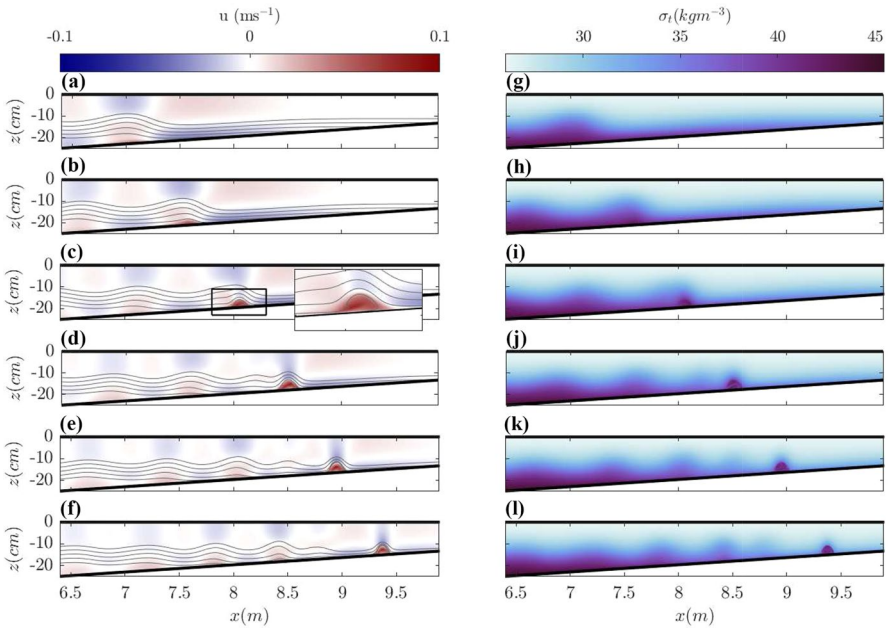

Fig. 4 Same as Fig. 2, but for a fissioning wave in the broad tanh stratification (Exp. Broad-10L). Time interval between images is $\Delta t = 9$s

relationships with these quantities are investigated here. For small incident waves, the number of pulses increase as the pycnocline thickness decreases. Meanwhile, as A_w increases, the number of pulses also increase, due to more energy being available to produce these waves (Fig. 6). However, as A_w passes the point at which pulses become unstable, the number of pulses produced rapidly decrease with increasing A_w, as increasing energy is lost to turbulent mixing and dissipation (Fig. 3). As the leading order control on upslope fluid transport, the number of pulses is affected by both incident amplitude and by the stratification. Upslope fluid transport will also be indicated by the amplitude(A_p) and width (λ_p) of the pulses (Fig. 7). Across all three stratifications, the maximum wave amplitude of the first pulse is directly proportional to the incident wave amplitude (Fig. 7a), and this relationship is very similar between stratifications, with the surface stratification producing marginally smaller amplitude pulses. For the broad tanh stratification, the pulse amplitude can be described as $A_p = 0.812A_w + 0.0087$, whilst for the surface and thin stratifications, pulse amplitude is $A_p = 0.900A_w - 0.0038$ and $A_p = 0.9389A_w + 0.0046$ respectively. Figure 9a–c shows the role of this relationship, that non-dimensionalised pulse amplitude (A_p/A_w) in the broad tanh stratification is lower for larger waves in the broad tanh stratification, whilst in the other stratifications, this A_p/A_w is very similar between simulations. Similar relationships exist between incident wave amplitude and pulse width, λ_p (Fig. 7c), which show increasing pulse width with wave amplitude, and also with pulse amplitude A_p. λ_p is larger for the waves in the broad tanh stratification, likely due to small non-linearity parameters in this stratification, but indicative of increased (initial) fluid transport for those waves.

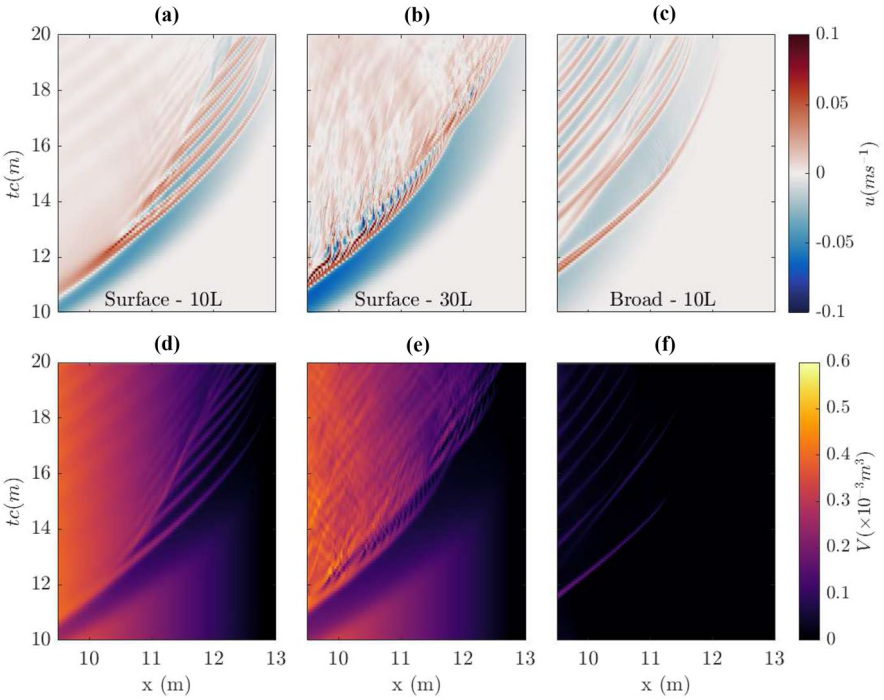

Fig. 5 Hovmoller plots of near-bed horizontal velocity (**a**–**c**) and volume of fluid under the $\rho = \rho_0 + \Delta\rho/2$ contour, V, (**d**–**f**) for the three waves shown in Figs. 2 (left), 3 (center) and 4 (right). Note the x-scale differs to that used in Figs. 2,3 and 4 in order to observe longer time and spatial scales required to capture the evolution of the pulses

3.2 Pulse evolution and degeneration

Upslope fluid transport in all stratifications is dominated by the passage of dense pulses, which present as red curves (upslope flow) across Fig. 5a–c interspersed with slower downslope (blue) regions. Each pulse transports a new parcel of dense fluid upslope, although the volume transported in each decreases (Fig. 5d–f). The presence of smaller-scale flow features at higher incident wavelengths is also reflected in the upslope fluid transport signal (Fig. 5).

Leading pulse propagation speed (at the time when A_p is maximum), c_p, appears to scale with A_p (Fig. 7e), until (for the surface and thin tanh stratifications) the transition to the more turbulent/unstable regime reduces the propagation speed of the pulse. The negative relationship between c_w and c_p in the broad tanh stratification (Fig. 7d) is explained by the fact that in this stratification, wave speed decreases as A_w increases. As such, higher c_w represent smaller amplitude incident waves, which in turn produce smaller amplitude pulses (A_p) (Fig. 7a). Therefore, it appears that pulse velocity is more closely determined by A_p (indicating pulses propagate as ISWs of elevation) than by their initial velocity (c_w). Furthermore, Fig. 7d shows that the actual wave propagation speed (c_w) is slower than the linear long wave speed for the broad tanh stratification, indicating that waves in this stratification are not ISWs, in part responsible for the different process of pulse formation in this stratification.

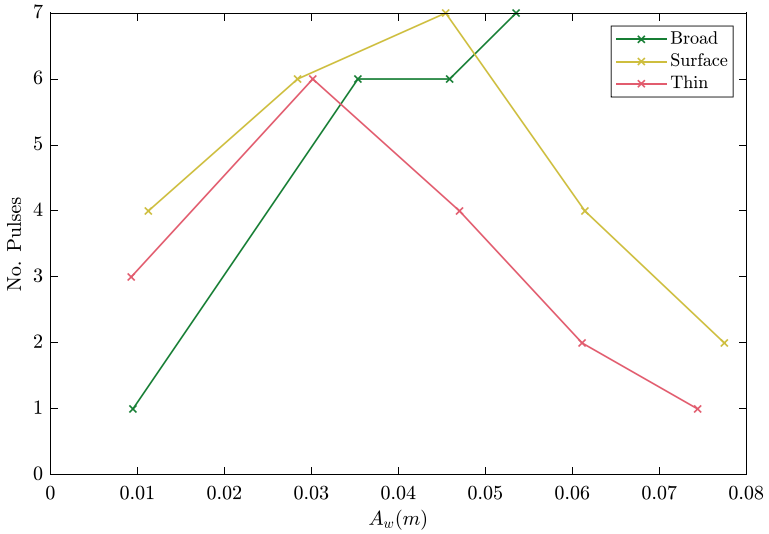

Fig. 6 Number of pulses identified from an incident wave during the simulation as a function of wave amplitude, A_w, for each of the three stratification types

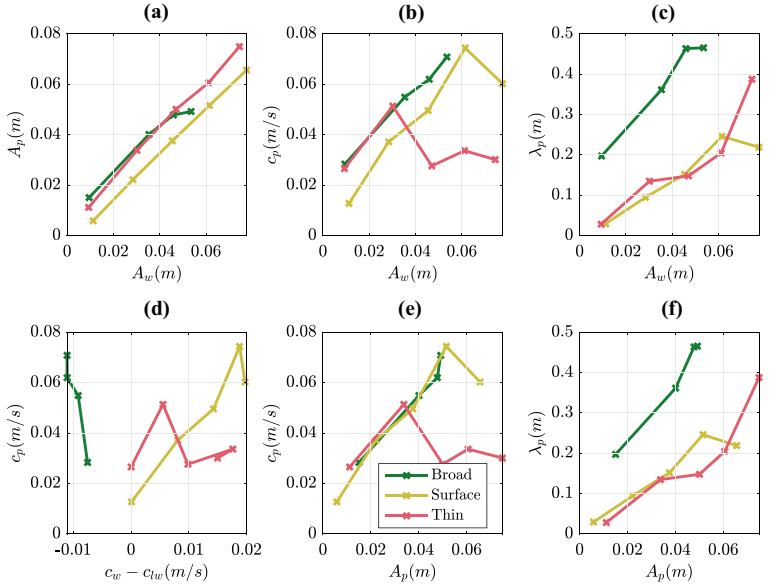

Fig. 7 Plots to show relationship between wave amplitude, wavelength, and speed, and the same properties of the leading pulse at the time at which pulse amplitude is maximum for each of the three stratifications. **a** Wave Amplitude, A_w, against Pulse Amplitude, A_p; **b** A_w against pulse speed, c_p; **c** A_w against pulse width (wavelength) λ_p; **d** Wave speed - linear long wave speed, $c_w - c_{lw}$ against c_p; **e** A_p against c_p; and f) A_p against λ_p

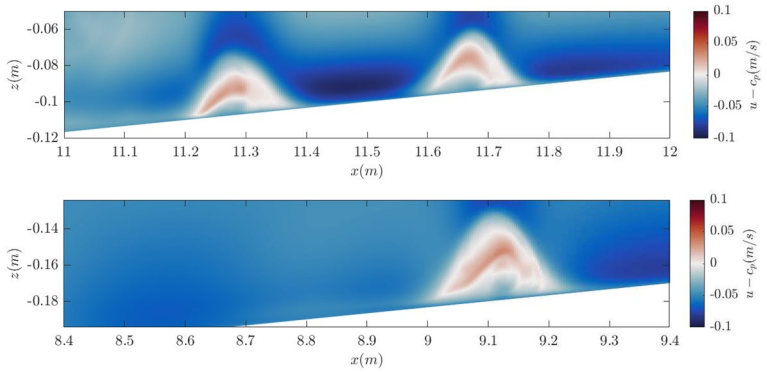

Fig. 8 Plot of flow velocity u relative to the pulse propagation speed (c_p) for the pulse shown in Fig. 2 (top) at same time as Fig. 2d, and 4 (bottom) at same time as Fig. 4e

As the pulses form, they are initially symmetrical, (Fig. 2b inset), however as they propagate upslope, the front face steepens, and the rear face extends (Figs. 2d, e, j, 8). This same steepening was previously observed in the thin tanh stratification [43]. During this process, pulses of dense fluid are carried upslope beyond the undisturbed height (Fig. 2i, j). After formation, the pulses in all stratifications slow down, and lose both amplitude and width (Fig. 9). As previously observed by Ghassemi et al [28], the pulse amplitude decreases linearly across all stratification types (Fig. 9a–c). Within stratifications, the rates of the degeneration are very similar between different sized waves 9d–f), but vary between stratifications, with the amplitude of pulses in the broad tanh stratification decreasing faster. Likewise, the pulses lose amplitude and wavelength at similar rates. Whilst the pulses propagate upslope, there is a substantial quasi trapped core (red areas) but the core is asymmetric in the along slope direction, with clear "leakiness" (blue) near the back where fluid is continually lost from the rear of the pulse (Fig. 8). This can be seen as the overall volume of dense fluid in the pulse decreasing upslope and through time (Fig. 5d–f).

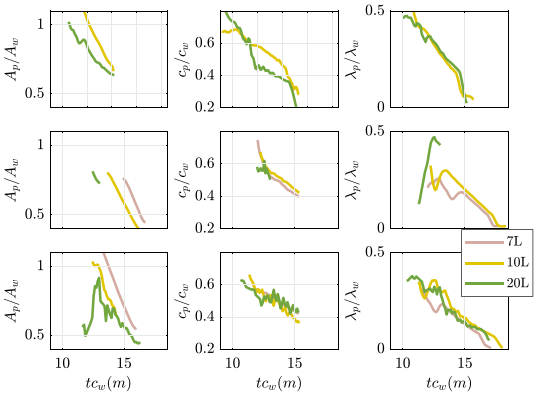

Fig. 9 Time-evolution of pulse properties A_p (left) c_p (centre) and λ_p (right), each non-dimensionalised by their equivalent wave property (A_w, c_w, and λ_w respectively) for the broad tanh (top), surface (middle) and thin tanh (bottom) stratifications

4 Discussion and conclusion

Here, fission of ISWs in stratifications deviating from a three-layer approximation has been investigated, for the first time in detail using a numerical model at the laboratory scale, which allows a full investigation into the time evolution of these structures which is difficult to achieve with field observations. Similar stratifications to those studied here have been investigated in the field [e.g. 44] highlighting the need for idealised studies to consider different stratifications to simply the three-layer stratification in order to fully understand the dynamics. However, despite the differences between stratification types for other wave breaking types, the transition between thin tanh and surface stratifications is found to have minimal impact on the fissioning of ISWs, in terms of pulse formation, structure and evolution. Additionally, the process by which pulses are formed by fission in numerical simulations in this study both for the surface and thin tanh stratifications are very similar to previously published numerical [19] and experimental works in the thin tanh stratification [28]. Shoaling waves in the broad tanh stratification undergo a considerably different process of fissioning, emerging instead from an elevation wave, and remained non-turbulent at all incident wave amplitudes, despite the structure of the pulse being similar to in the other stratifications.

Whilst the use of 3-D simulations in studies of internal wave shoaling would be desirable in order to resolve lobe-cleft instabilities and lateral variability, such simulations over this length of wave tank are too computationally expensive. Furthermore, past studies have highlighted the qualitative similarity of wave breaking in 2-D and 3-D simulations during the phases of shoaling studied here (the approach to the slope, breaking event, and start of up-slope propagation) [29, 34, 45]. Following on from these studies, it is expected that lateral variability and instabilities (which form only in 3-D simulations) would impact on the degeneration process of the pulses formed by fission.

Pulses formed by fission (in all stratification types) are single ISW-like pulses which propagate upslope, in comparison to boluses produced by other wave shoaling types (such as collapsing or surging) as studied by Vieira and Allshouse [30], Allshouse and Swinney [31], which exist as a parcel of fluid which travels in a manner more similar to a gravity current. In particular, Vieira and Allshouse [30] identified three bolus structures (ball, hook and slivers), which do not appear to correspond to the pulses produced by fission, indicating such features are dynamically different based on the process of shoaling that formed them.

Numerous field observations have detailed the process by which ISWs of depression fission into pulses propagating upslope due to the polarity reversal process [e.g. 22, 23]. Orr and Mignerey [22] detail the initial lengthening of the front face of the leading wave (as in Fig. 2a), followed by the formation of waves of elevation which advance through the rear of the leading wave of depression (as in Fig. 2b,c), in a stratification that is approximated by the surface stratification (see their Fig. 8). Comparisons between ADCP velocity fields of the pulses propagating upslope (their Fig. 12) and Fig. 2d, show striking similarity in the wave and pulse-induced velocity fields. The present observations are also in strong agreement with the observations of Shroyer et al [23] as the incident waves pass through the turning point and become internal solitary waves of elevation. The evolution of these pulses has also been documented in the field by Jones et al [25], Richards et al [44]. Velocity structures shown by Richards et al [44] Fig. 9 are in good agreement with the trains of pulses seen in this study, whilst Jones et al [25] report very active cores within the pulses, in contrast to this study. Richards et al [44] reported upslope advection by the wave of

turbulent fluid locally produced by fissioning internal waves. In this study, instabilities displayed by larger incident waves upon fissioning in the surface and thin tanh stratifications, and in particular, the vortices shed from the rear of the pulse, also leave behind turbulent fluid, which may form part of the process observed by Richards et al [44], although difference in scales (with a factor 50-100 difference in Reynolds number) impairs these comparisons. Such a process may be an important source of energy for mixing and dissipation along the slope and shelf.

Confirming that degeneration of pulses remains linear in three different stratifications is indicative that prior results [e.g. 28] will hold true in a range of real-world situations. As this degeneration occurs by the loss of fluid from the rear of the pulse, the rate at which it occurs has implications for the transport of bottom waters onto the shelf, which in turn, may impact on the benthic ecology. The three-dimensional structure of fissioning waves, in particular lobe-cleft instability was identified by Ghassemi et al [28], and would alter the mixing of the pulse with surrounding fluid.

Whilst the pulse structure and evolution is similar between the stratifications investigated in this study, the impact of the process of fissioning on ecosystems is still dependent on stratification. Variability in the number of boluses produced by waves in different stratifications (Fig. 6) is an important factor in upslope transport of fluid, and internal-wave derived energy. The time evolution of density (presented here as a "normalised density") at the bottom boundary for a fixed slope location is used to indicate transport of lower-layer water, and represent measurements by a virtual mooring (similar to the near-bottom temperature measurements in Richards et al [44], their Fig. 9), which in an oceanographic setting is typically cold and nutrient rich. Whilst the upslope transport is not permanent, and the dense fluid moves back downslope (Fig. 5), variability in temperature has previously been identified as an important factor for the health of benthic ecosystems Reid et al [2]. In all stratifications, an initial decrease in normalised density is observed as the incoming wave draws down fluid from the upper layer (Fig. 10). However, the formation of pulses brings dense (lower-layer) water upslope, in doing so modifying the water properties at that location. The overall change in density at the lower boundary is greatest for the largest amplitude waves (Fig. 10a–c). Between stratifications, the total change in density (relative $\delta\rho$) increases between broad tanh to surface, and further to thin tanh stratification, due to lower density gradients $\left(\frac{\delta\rho}{\delta z}\right)$. These pulses bring kinetic energy upslope, each pulse associated with a peak in the kinetic energy on the slope (Fig. 10). The impact of this is greatest for the broad stratification (Fig. 10d).

The fission of internal solitary waves over gentle, and crucially, geophysically realistic slopes forms coherent pulses of dense fluid, which in other contexts are also referred to as cold pulses, or boluses. Such pulses of fluid can be a significant source of nutrients and relief from excess heat to benthic ecosystems [2, 4], and understanding the role of stratification (which varies both spatially and seasonally) on the behaviour of these pulses is therefore important. Although the form of the pulse produced by fission is similar across three very different stratifications studied here, for the broad stratification, the pulse formation process does vary. Pulses in the broad stratification propagate slower, and disintegrate faster than in other stratifications. Whilst idealised studies remove the potential impacts of other ocean processes (e.g. the surface tide or eddies), here we show that in such idealised conditions unstable fissioning can also be found, producing pulses of turbulent fluid and advecting this turbulent fluid upslope, inducing mixing and dissipation further upslope than the energy source.

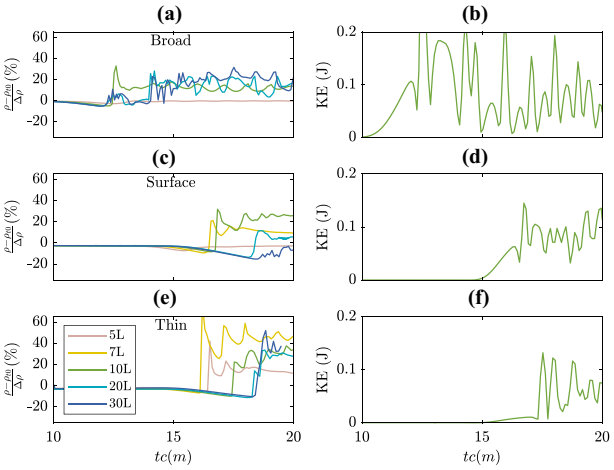

Fig. 10 Timeseries of normalised density (left) and kinetic energy (KE, right) at the bottom for the point where the slope intersects with the pycnocline location (left); Shown for each of the stratifications, broad tanh (top), surface (middle) and thin tanh (bottom), with time normalised by wave speed, c. For clarity only the 10L wave is shown for the KE plots

Supplementary Information The online version contains supplementary material available at https://doi.org/10.1007/s10652-022-09894-x.

Acknowledgements This work was supported by the Natural Environment Research Council (NERC) funded ONE Planet Doctoral Training Partnership (S.H.E., Grant Number [NE/S007512/1]). This research made use of the Rocket High Performance Computing service at Newcastle University. Prof Peter A Davies is thanked for introducing this rich and fascinating area of research to MC and providing invaluable support and mentorship to all three authors. Two anonymous referees are thanked for contributions to this manuscript.

Data availability Upon acceptance, all model data for this study will be available at https://doi.org/10.25405/data.ncl.c.5791673. The SPINS model and processing code is available via the user guide https://wiki.math.uwaterloo.ca/fluidswiki/index.php?title=SPINS_User_Guide.

References

1. Grue J, Jensen A, Rusas PO et al (1999) Properties of large-amplitude internal waves. J Fluid Mech 380:257–278. https://doi.org/10.1017/S0022112098003528
2. Reid EC, DeCarlo TM, Cohen AL et al (2019) Internal waves influence the thermal and nutrient environment on a shallow coral reef. Limnol Oceanogr 64(5):1949–1965. https://doi.org/10.1002/lno.11162
3. McPhee-Shaw EE, Siegel DA, Washburn L et al (2007) Mechanisms for nutrient delivery to the inner shelf: observations from the Santa Barbara Channel. Limnol Oceanogr 52(5):1748–1766. https://doi.org/10.4319/lo.2007.52.5.1748
4. Green RH, Jones NL, Rayson MD et al (2019) Nutrient fluxes into an isolated coral reef atoll by tidally driven internal bores. Limnol Oceanogr 64(2):461–473. https://doi.org/10.1002/lno.11051

5. Safaie A, Silbiger NJ, McClanahan TR et al (2018) High frequency temperature variability reduces the risk of coral bleaching. Nat Commun 9(1):1–12. https://doi.org/10.1038/s41467-018-04074-2
6. Helfrich KR, Melville WK (2006) Long nonlinear internal waves. Annu Rev Fluid Mech 38(1):395–425. https://doi.org/10.1146/annurev.fluid.38.050304.092129
7. Boegman L, Stastna M (2019) Sediment resuspension and transport by internal solitary waves. Annu Rev Fluid Mech 51(1):129–154. https://doi.org/10.1146/annurev-fluid-122316-045049
8. Huang X, Chen Z, Zhao W et al (2016) An extreme internal solitary wave event observed in the northern South China Sea. Sci Rep 6(1):30041. https://doi.org/10.1038/srep30041
9. Lamb KG (2014) Internal wave breaking and dissipation mechanisms on the continental slope/shelf. Annu Rev Fluid Mech 46(1):231–254. https://doi.org/10.1146/annurev-fluid-011212-140701
10. Rayson MD, Jones NL, Ivey GN (2019) Observations of large-amplitude mode-2 nonlinear internal waves on the australian north west shelf. J Phys Oceanogr 49(1):309–328. https://doi.org/10.1175/JPO-D-18-0097.1
11. da Silva JC, Buijsman MC, Magalhaes JM (2015) Internal waves on the upstream side of a large sill of the Mascarene Ridge: a comprehensive view of their generation mechanisms and evolution. Deep Sea Res Part 1 Oceanogr Res Pap 99:87–104. https://doi.org/10.1016/j.dsr.2015.01.002
12. Grue J (2005) Generation, propagation, and breaking of internal solitary waves. Chaos 15(3):037110. https://doi.org/10.1063/1.2047907
13. Boegman L, Ivey GN, Imberger J (2005) The degeneration of internal waves in lakes with sloping topography. Limnol Oceanogr 50(5):1620–1637. https://doi.org/10.4319/lo.2005.50.5.1620
14. Michallet H, Ivey GN (1999) Experiments on mixing due to internal solitary waves breaking on uniform slopes. J Geophys Res Oceans 104(C6):13467–13477. https://doi.org/10.1029/1999jc900037
15. Sutherland BR, Barrett KJ, Ivey GN (2013) Shoaling internal solitary waves. J Geophys Res Oceans 118(9):4111–4124. https://doi.org/10.1002/jgrc.20291
16. Aghsaee P, Boegman L, Lamb KG (2010) Breaking of shoaling internal solitary waves. J Fluid Mech 659:289–317. https://doi.org/10.1017/S002211201000248X
17. Nakayama K, Sato T, Shimizu K et al (2019) Classification of internal solitary wave breaking over a slope. Phys Rev Fluids 4(1):014801. https://doi.org/10.1103/PhysRevFluids.4.014801
18. Arthur RS, Koseff JR, Fringer OB (2017) Local versus volume-integrated turbulence and mixing in breaking internal waves on slopes. J Fluid Mech 815:169–198. https://doi.org/10.1017/jfm.2017.36
19. Xu C, Stastna M (2020) Instability and cross-boundary-layer transport by shoaling internal waves over realistic slopes. J Fluid Mech. https://doi.org/10.1017/jfm.2020.389
20. Cacchione DA, Pratson LF, Ogston AS (2002) The shaping of continental slopes by internal tides. Science 296(5568):724–727. https://doi.org/10.1126/science.1069803
21. Wallace BC, Wilkinson DL (1988) Run-up of internal waves on a gentle slope in a two-layered system. J Fluid Mech 191:419–442. https://doi.org/10.1017/S0022112088001636
22. Orr MH, Mignerey PC (2003) Nonlinear internal waves in the South China Sea: observation of the conversion of depression internal waves to elevation internal waves. J Geophys Res 108(C3):3064. https://doi.org/10.1029/2001JC001163
23. Shroyer EL, Moum JN, Nash JD (2009) Observations of polarity reversal in shoaling nonlinear internal waves. J Phys Oceanogr 39(3):691–701. https://doi.org/10.1175/2008JPO3953.1
24. St Laurent L, Simmons H, Tang TY et al (2011) Turbulent properties of internal waves in the South China Sea. Oceanography 24(4):78–87. https://doi.org/10.5670/oceanog.2011.96
25. Jones NL, Ivey GN, Rayson MD et al (2020) Mixing driven by breaking nonlinear internal waves. Geophys Res Lett 47(19):e2020GL089591. https://doi.org/10.1029/2020GL089591
26. Moum JN, Farmer DM, Smyth WD et al (2003) Structure and generation of turbulence at interfaces strained by internal solitary waves propagating shoreward over the continental shelf. J Phys Oceanogr 33(10):2093–2112
27. Shroyer EL, Moum JN, Nash JD (2010) Energy transformations and dissipation of nonlinear internal waves over New Jersey's continental shelf. Nonlinear Process Geophys 17(4):345–360. https://doi.org/10.5194/npg-17-345-2010
28. Ghassemi A, Zahedi S, Boegman L (2022) Bolus formation from fission of nonlinear internal waves over a mild slope. J Fluid Mech. https://doi.org/10.1017/jfm.2021.1033
29. Arthur RS, Fringer OB (2014) The dynamics of breaking internal solitary waves on slopes. J Fluid Mech 761(2):360–398. https://doi.org/10.1017/jfm.2014.641
30. Vieira GS, Allshouse MR (2020) Internal wave boluses as coherent structures in a continuously stratified fluid. J Fluid Mech 885:A35. https://doi.org/10.1017/jfm.2019.993
31. Allshouse MR, Swinney HL (2020) Dependence of internal wave bolus transport on pycnocline thickness. Geophys Res Lett 47(14):e2020GL086952. https://doi.org/10.1029/2020GL086952

32. Maderich VS, Van Heijst GJ, Brandt A (2001) Laboratory experiments on intrusive flows and internal waves in a pycnocline. J Fluid Mech 432:285–311. https://doi.org/10.1017/s0022112000003323
33. Vlasenko V, Stashchuk N, Hutter K (2005) Baroclinic Tides. Cambridge University Press, Cambridge. https://doi.org/10.1017/CBO9780511535932
34. Hartharn-Evans SG, Carr M, Stastna M et al (2022) Stratification effects on shoaling internal solitary waves. J Fluid Mech. https://doi.org/10.1017/jfm.2021.1049
35. Walter RK, Phelan PJ (2016) Internal bore seasonality and tidal pumping of subthermocline waters at the head of the Monterey submarine canyon. Cont Shelf Res 116:42–53. https://doi.org/10.1016/j.csr.2016.01.015
36. Moum JN, Klymak JM, Nash JD et al (2007) Energy transport by nonlinear internal waves. J Phys Oceanogr 37(7):1968–1988. https://doi.org/10.1175/JPO3094.1
37. Subich CJ, Lamb KG, Stastna M (2013) Simulation of the Navier-Stokes equations in three dimensions with a spectral collocation method. Int J Numer Methods Fluids 73(2):103–129. https://doi.org/10.1002/fld.3788
38. Harnanan S, Stastna M, Soontiens N (2017) The effects of near-bottom stratification on internal wave induced instabilities in the boundary layer. Phys Fluids 29(1):016602. https://doi.org/10.1063/1.4973502
39. Deepwell D, Stastna M, Carr M et al (2017) Interaction of a mode-2 internal solitary wave with narrow isolated topography. Physics of Fluids 29(7):076601. https://doi.org/10.1063/1.4994590
40. Lamb KG, Nguyen VT (2009) Calculating energy flux in internal solitary waves with an application to reflectance. J Phys Oceanogr 39(3):559–580. https://doi.org/10.1175/2008JPO3882.1
41. Carr M, Davies PA (2006) The motion of an internal solitary wave of depression over a fixed bottom boundary in a shallow two-layer fluid. Phys Fluids 18(1):016601. https://doi.org/10.1063/1.2162033
42. Bogucki DJ, Redekopp LG, Barth J (2005) Internal solitary waves in the coastal mixing and optics 1996 experiment: multimodal structure and resuspension. J Geophys Res C Oceans 110(2):1–19. https://doi.org/10.1029/2003JC002253
43. Xu C, Subich C, Stastna M (2016) Numerical simulations of shoaling internal solitary waves of elevation. Phys Fluids 28(7):76,601. https://doi.org/10.1063/1.4958899
44. Richards C, Bourgault D, Galbraith PS et al (2013) Measurements of shoaling internal waves and turbulence in an estuary. J Geophys Res Oceans 118(1):273–286. https://doi.org/10.1029/2012JC008154
45. Xu C, Stastna M, Deepwell D (2019) Spontaneous instability in internal solitary-like waves. Phys Rev Fluids 4(1):014805. https://doi.org/10.1103/PhysRevFluids.4.014805